metals

Article

The Effect of Welding Mode Parameters on the Operational Properties of Flexible Compensating Elements Made of Austenitic Stainless Steels

Vitaliy Petrovich Ivanov [1], Elena Vladimirovna Lavrova [1], Fedor Viktorovich Morgay [1], Dmitry Pavlovich Ilyashenko [2,3,*] and Viktoria Yuryevna Ivashchenko [1]

[1] Pryazovsky State Technical University, Universitetskaya 7, Mariupol 287555
[2] National Research Tomsk Polytechnic University, Building 30, Lenin Ave., Tomsk 634050, Russia
[3] Institute of Strength Physics and Materials Science of Siberian Branch Russian Academy of Sciences, Academic Ave., 2/4, Tomsk 634055, Russia
* Correspondence: mita8@tpu.ru

Abstract: The paper investigates the effect of welding mode parameters on the uniformity of the deformation capacity of AISI 316 austenitic steel samples, namely, the influence of the welding current and purging gas consumption on the samples' ability to perceive the force of cold cupping. Punch diameters of 3 and 8 mm were employed for the Erikson test to establish the dependence of the purge gas flow rate on the depth of the hole before the formation of cracks. The conducted metallographic studies confirmed an increase in the homogeneity of the dendritic structure in the weld zone due to the redistribution of heat input, as well as the absence of uneven grains and a decrease in the spread of grain sizes, which were in the range of 0.068–0.045 mm. The study resulted in determining the optimal range of technological parameters for the manufacture of flexible expansion elements to ensure their high operational properties.

Keywords: flexible compensating elements; austenitic stainless steel; purging gas; flow rate; TIG-welding; strips extrusion

Citation: Ivanov, V.P.; Lavrova, E.V.; Morgay, F.V.; Ilyashenko, D.P.; Ivashchenko, V.Y. The Effect of Welding Mode Parameters on the Operational Properties of Flexible Compensating Elements Made of Austenitic Stainless Steels. *Metals* **2023**, *13*, 423. https://doi.org/10.3390/met13020423

Academic Editors: Dmitry A. Chinakhov and Hardy Mohrbacher

Received: 22 November 2022
Revised: 15 January 2023
Accepted: 15 February 2023
Published: 17 February 2023

1. Introduction

Previous research has shown that, in most cases, the corrosion destruction of flexible compensating elements (FCEs) is caused by the stress state arising from elastoplastic deformations during their manufacture and operation [1,2]. A high level of residual stresses and, accordingly, a decrease in elastic-plastic characteristics [3,4], as well as an increased level of structural inhomogeneity in welded seams and the heat-affected zone [5,6], lead to the destruction of the most loaded sections of these products during their operation (Figure 1). Additionally, factors such as the environment's composition [7,8] and the presence of media that contain chloride [9], might hasten the development of local foci of corrosion and reduce FCEs' service life.

Studies on the causes of local corrosion-mechanical damage in the welded seams and the heat-affected zone of structures made of austenitic steels have demonstrated a significant influence of the microstructure and mechanical characteristics [10,11], as well as the welding process parameters [12,13], on the performance properties.

According to the research findings presented in [14], welding mode parameters significantly affect the mechanical characteristics of welded joints made of austenitic stainless steels. Importantly, a simultaneous increase in the main welding parameters, such as welding speed and welding current, coupled with a constant level of heat input, lead to an improvement in the weld metal's mechanical properties due to a change in the welded joint's microstructure. The tensile strength and relative elongation of the weld metal could be increased as a result, thus increasing the level of equal strength of the welded joint [14].

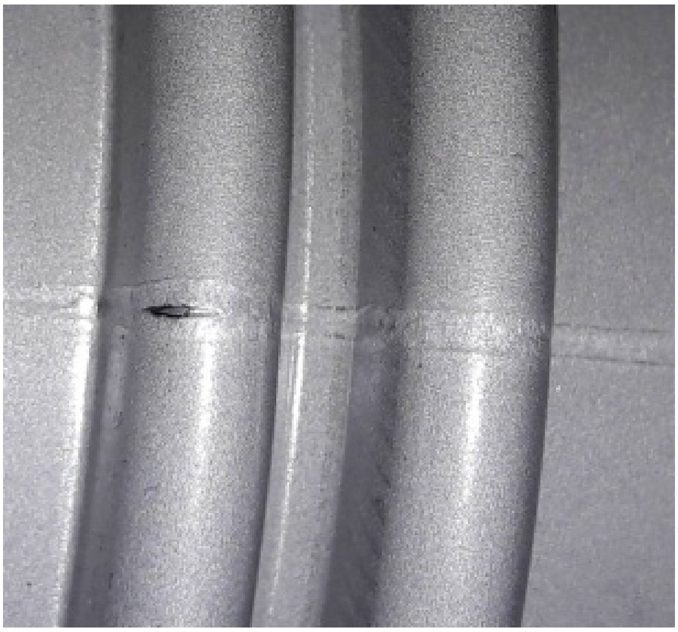

Figure 1. Destruction of the bellows expansion joint along the axis of the weld.

The studies demonstrate that for austenitic materials, the pulsed welding mode has an advantage over the continuous one in terms of the microstructural and mechanical properties of welded joints and deposited layers. The results of the experiments led the authors of [15] to the conclusion that the best microstructural and mechanical qualities of the weld metal can be obtained using the pulsed mode of metal transfer. Furthermore, the study [16] has discovered that, due to the grain refinement that occurs in the fusion zone, the pulsed current method increases the tensile properties of AZ31B magnesium alloy welds unlike continuous current welds. A comparable result is achieved by reducing the heat input into the weld and slag pools and decreasing their fluidity, as was the case in [17] when applying controlled mechanical transfer during surfacing with austenitic strip electrodes on pearlitic steel.

Similar conclusions were made in [18] for the case of plasma arc weld joints made of 316L austenitic stainless steel and for the case of welded joints of 12Cr18Ni10Ti austenitic steel [19]. In [20], the use of controlled mechanical impacts on the electrode surfacing with austenitic materials was proposed as a method to improve the mechanical properties of the HAZ.

According to [21,22], the properties of welds in 304L austenitic steel are improved by a decrease in heat input, and this effect is said to be more evident as the metal thickness decreases. In [23], the refractory particles in the weld pool are used to boost the centers of crystallization and create a suitable weld microstructure to control the structure formation and mechanical properties of the 316 steel's microstructure.

To reach a state of equivalent strength, the degree of heat input into the weld pool and base metal must, however, offer consistent and stable penetration along the entire length of the weld. Furthermore, the thermal cycle of welding is one of the main driving forces for the processes of recrystallization and grain growth occurring in the heat-affected zone, which is the direct cause for local areas of a decrease in the level of mechanical properties in this area. [24]. Additionally, the effect of the welding-generated δ-ferrite on the mechanical properties and corrosion resistance must be considered when choosing the welding mode parameters for 300-series austenitic steels, particularly for the most popular AISI 304 steel [25,26].

The potential sources of the issues that occur during the deformation of welded FCE blanks were analyzed, among them being the compliance of the base and welding materials, the welding mode, and other technological parameters' compliance with the normative documentation requirements. The chemical composition of the materials was analyzed, as well as the effect of the welding modes on the mechanical characteristics of welded junctions. To achieve this, various samples were created, and their welding was carried out using various mode parameters. Each group had a total of five samples.

Accordingly, the study was conducted to determine how different welding current and speed values in TIG welding modes without filler material affected the mechanical properties of welded samples made of the austenitic steel grades AISI 304 and AISI 316. After the samples were cut, tensile tests were performed to determine how the welding mode affected the strength and plasticity of the welded joints. A data acquisition board connected to a test stand was used to gather mechanical properties, while devices installed on the welding machine were used to gather welding mode parameters. The results of the samples' mechanical tests are listed in Table 1.

Table 1. Results of the mechanical tests.

No.	Material	Welding Current I, (A)	Arc Voltage U, (V)	Welding Speed v, (mm/s)	Mechanical Properties		
					$\sigma_{0.2}$, MPa	σ_T, MPa	δ, %
1	AISI 304	10–14	12–14	16	215	518	46
2	AISI 304	15–18	12–14	17	210	522	44
3	AISI 304	18–22	10–12	18	201	540	45
4	AISI 316	10–14	10–12	16	220	528	48
5	AISI 316	15–18	10–12	17	234	522	43
6	AISI 316	18–22	10–12	18	237	530	45

The results of the mechanical tests of specimens made of austenitic steels AISI 304 and AISI 316 showed that the scatter in the values of mechanical properties was small and, in general, corresponded to the standard indicators for these steels. The destruction of the samples occurred both along the base metal and along the weld zone, which indicates a sufficient equal strength of the welded joints. According to the analysis of the samples that failed along the welds, an increase in both the current strength and the welding speed (though to a smaller extent) increased the strength of the welded joint within the investigated modes (Table 1 shows the average values of the samples' mechanical characteristics). This dependence is explained by the fact that the cross-sectional area of the weld grows as the welding current increases.

The obtained dependencies were more complicated for the plasticity properties of the samples that failed along the seam. For both steel grades, there was an observed zone of optimal welding mode parameters with the plastic characteristics higher than the average values for a group of samples. This observation allowed for the assumption that there was a maximum of plastic properties in this region of the welding mode parameters. This phenomenon was also confirmed in [1].

The study of the resistance of tapes made of austenitic steels AISI 304 and AISI 316, as well as welded samples of these materials against IGC, consisted in holding them in a boiling aqueous solution of copper sulfate and sulfuric acid, followed by metallographic control of sections. The working solution consisted of (50 $\pm$ 0.1) g of copper sulfate, (250 $\pm$ 3) cm^3 of sulfuric acid, (1000 $\pm$ 3) cm^3 of water. The added copper shavings ensured all-round contact with the samples and the absence of their contact with each other. The exposure time in the boiling solution was (8.00 $\pm$ 0.25) hours. After testing, the samples were removed from the solution, washed in running water, rinsed with distilled water, and dried with filter paper. Before the preparation of metallographic sections, the samples were stored in a desiccator.

Metallographic specimens were produced with diamond pastes of various dispersion levels according to the conventional procedure. The samples were electrolytically etched for 15 seconds at a voltage of 12 V in a solution of 20% ammonium sulfate to reveal the microstructure. Metallographic studies were conducted on a NEOPHOT 32 microscope at magnifications of ×250 and ×500.

The structure of the weld metal of the control sample is formed by crystals that grow through the axis of the weld during crystallization. The junction of two crystallization fronts in the center of the seam is an interweaving of the crystallite vertices. The microstructure of the weld metal is austenite and δ-ferrite, that of the HAZ and the base metal is austenite. The hardness of the weld metal, HAZ and base metal is H_{v1} (2740–2810) MPa, H_{v1} 2620 MPa, and H_{v1} 2580 MPa, respectively. The grain size is equal to 6–7 points for HAZ and 7 for base metal.

In the central part of the samples' seam, there are areas of a fine-grained structure. The microstructure of the weld metal is austenite and δ-ferrite, and that of the HAZ and base metal is austenite. In the HAZ, the grain size is 6 points. The precipitation of fine particles, probably chromium carbides, is observed at a distance of about 540 μm from the fusion line along the boundaries of austenite grains. The hardness of the weld metal, HAZ, and base metal is H_{v1} (2120–2130) MPa, H_{v1} (2240–2280) MPa, and H_{v1} 2060 MPa, respectively. The base metal grain score is 7.

In the weld metal of the sample after the resistance testing against IGC, there is a misorientation of crystallites in the center; its microstructure is austenite and δ-ferrite. In the HAZ, the microstructure is austenitic. The hardness of the weld metal, HAZ, and base metal is H_{v1} 2450 MPa, H_{v1} (2130–2190) MPa, and H_{v1} 2060 MPa, respectively. The base metal grain score is 7, and the HAZ is 6. Fine particles, most likely chromium carbides, precipitated along the austenite grain boundaries at a distance of roughly 500 μm from the fusion line. Since there was no precipitation of chromium carbides along the grain boundaries in the tape's microstructure from which the sample was made, they are likely to have formed as a result of technological processes during the sleeve's production (welding, corrugating, etc.).

The microstructure of the tape samples used for the manufacture of welded samples before and after the resistance testing against IGC is austenitic, a rolling trace is visible, and the grain score is 7. The hardness of the control sample is H_{v1} (2130–2150) MPa; that of the sample after the resistance testing against IGC is H_{v1} 2280 MPa. Generally, the metal displayed the precipitation of chromium carbides at the grain boundaries.

The results of metallographic studies revealed that welded joints and tapes for the manufacture of FCE are not subject to IGC. However, the release of fine particles along the boundaries of grains and twins can contribute to the increased sensitivity of the metal to intergranular corrosion during operation.

Additionally, we looked at how plastic deformation affected the steels' resistance to corrosion. In this instance, the distortion of the samples ranged from 0% to 70%. The high flow rate of these steels' electrochemical corrosion in a 60% NaCl solution led to its application as a corrosion medium. Figure 2 illustrates the relationship between the degree of deformation and the change in the mass of the steel samples under investigation.

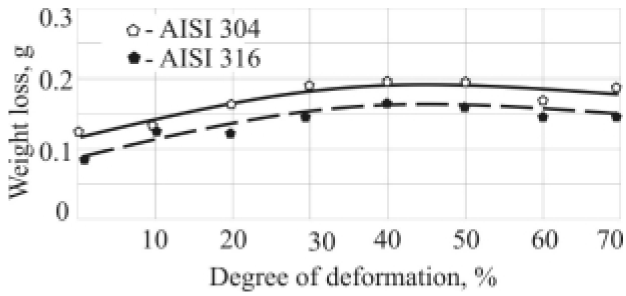

Figure 2. The study results of the electrochemical corrosion dependence on the degree of the samples' deformation.

The study's findings demonstrate that the degree of deformation affects the tested steels' level of corrosion resistance. Concurrently, high values of the corrosion resistance index are noted throughout the examined range. The full-scale testing conducted during product manufacturing, however, revealed that, despite their tendency to decline, formation defects continued to occur. Since no corrosion centers were found throughout the testing, other variables influencing the heat input into the welded joints of the FCE blanks were examined.

We also included provisions for the fact that the temperature regime in the weld zone during welding in a shielding gas environment depends on the flow rate of the purge (root shielding) gas if the technological process requires its supply.

Researchers examined the purge gas influences on the 304H [27] and 308L [28] welds' corrosion, mechanical, and microstructural properties. Additionally, it has been found that the humidity and purity of the purge gas have a substantial impact on the microstructure and mechanical properties of GTA welds [29]. With the exception of tensile tests, standard mechanical tests rarely apply to FCE because most of these items are manufactured from thin austenitic strips, sheets, and wires. Furthermore, the impact of the purge gas flow rate on the welded billets' plastic deformation capacity has not been researched.

Consequently, this work aimed to identify the welding mode parameters that would enable 300 series of austenitic steels to be used for the production of welded joints with the best mechanical and structural performance while using the optimal amount of heat.

2. Methods of Research

To meet the stated study objective, we conducted tests on the mechanical characteristics of samples of the welded joints made of AISI 316 austenitic steel with a thickness of 0.25 mm.

At various values of the mode parameters, the TIG method was employed to weld the samples without the use of a filler material (Table 2).

Table 2. Parameters of changing the welding modes of the AISI 316Lsteel samples.

No. Series of Samples	Metal Thickness, (mm)	Welding Current I, (A)	Arc-Voltage U, (V)	Welding Speed v, (mm/s)	Argon Consumption, (lpm)	Purging Argon Flow Rate Range q, (lpm)
1	0.25	12	12–14	16	14–16	8–18 in steps of 2
2	0.25	14	12–14	16	14–16	10–18 in steps of 2
3	0.25	16	10–12	17	14–16	8–18 in steps of 2
4	0.25	18	10–12	17	14–16	10–18 in steps of 2
5	0.25	20	10–12	18	14–16	12–18 in steps of 2
6	0.25	22	10–12	18	14–16	8–18 in steps of 2
7	0.25	24	10–12	18	14–16	10–18 in steps of 2

The geometric parameters of the welded seams were discovered to match the criteria of the technical documentation and the relevant standards for every analyzed welding mode in each set of samples.

However, the appearance of the welds produced using various mode values varied noticeably, both on the top and the root side. Figure 3 displays the samples of the welds performed at lower welding currents (12–18 A) and purging gas flow rates (8–14 lpm).

Zeiss optical microscope (NEOPHOT 21) was employed for microhardness tests and metallographic studies of the structure to clarify the mechanism by which the welding mode parameters affect the characteristics of the weld zone and the heat-affected zone and to predict the behavior of the welded products during further cold deformation (corrugation).

The microhardness was first measured immediately around the weld for each sample, with no significant changes discovered. Then, the samples of AISI 316L steel obtained at various values of the variable parameters (see Table 2) of the welding mode were subjected to comparative metallographic investigations of the weld and heat-affected zones.

(**a**)

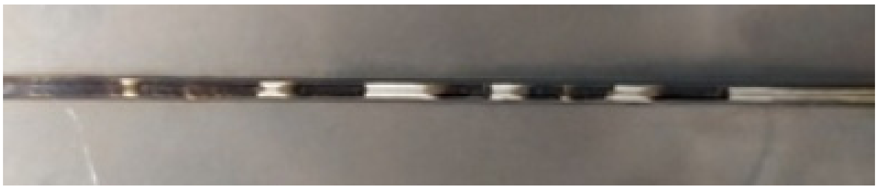

(**b**)

Figure 3. The weld seam top (**a**), and root (**b**) view, ×1.6. Mode parameters: I = 12–14 A; v = 17–18 mm/s; q = 8–14 lpm.

Higher levels of the welding mode's variable parameters (18–24 A and 14–18 lpm) resulted in smoother, shiny-surfaced seams with almost no color change (Figure 4).

(**a**)

(**b**)

Figure 4. The weld seam top (**a**), and root (**b**) view, ×1.6. Mode parameters: I = 18–24 A; v = 17–18 mm/s; q = 12–18 lpm.

In the weld zone, a dendritic structure of the crystallized metal with pronounced liquation is observed in the microstructure of the samples obtained at lower values of the current strength and purging gas flow rate. This structure is discernible in the form of darker areas in the interdendritic regions and lighter bodies of the dendrites themselves. While the seam zone is represented by columnar, more extended, and larger crystals, the zone of liquid crystallized metal at the point of contact with the unmelted layer has a more dispersed dendritic structure (Figure 5). At the lower boundary of the fusion zone, there are additional single inclusions whose composition and origin are unknown.

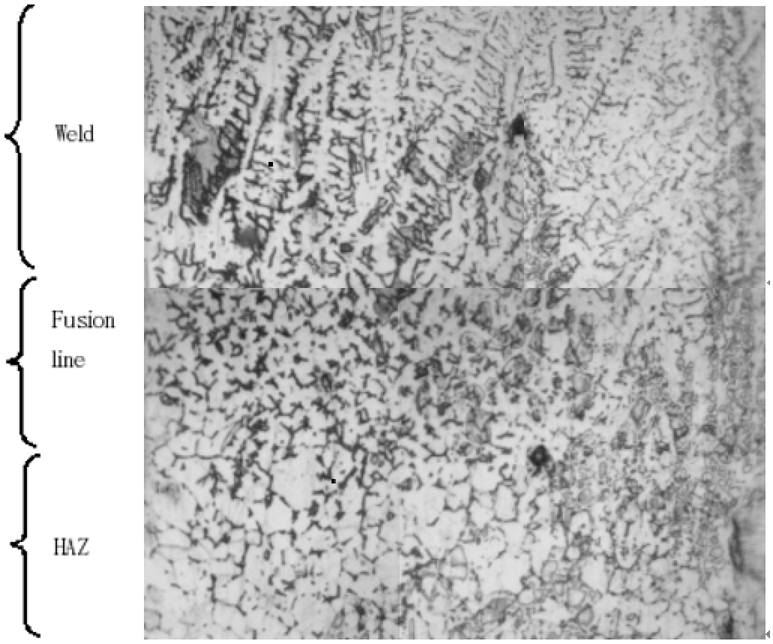

Figure 5. Collage of microstructures of a welded joint made of AISI 316L steel at low values of mode parameters (×500).

The secant approach was used to estimate the grain sizes in the heat-affected zone to evaluate the impact of energy input. In the HAZ, an austenite grain with a consistent etching is observed. The individual grains have diameters between 0.095 and 0.075 mm, according to measurements, while most grains are between 0.072 and 0.055 mm in size.

A more homogeneous dendritic structure is observed in the seam zone at gas flow rates of 15–18 lpm and amperage of 16–20 A. The grain is more uniform in size and lacks any graininess in the heat-affected zone compared to the preceding instance. The range of grain size is 0.068 to 0.045 mm. The average grain size of the base metal is 0.030 mm.

Microstructural studies show that, in this instance, the fusion line is formed without obvious segregation (Figure 6a), and the HAZ has a granular and uniform structure (Figure 6b).

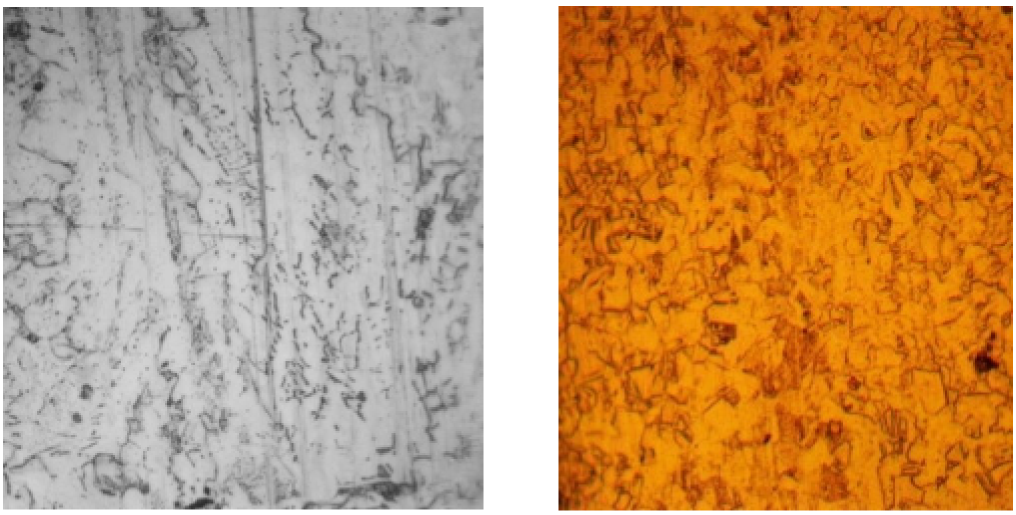

(**a**) (**b**)

Figure 6. The microstructure of the fusion zone (**a**) and HAZ (**b**) at higher values of the mode parameters (×500).

The uniformity of the plasticity characteristic distribution, which is difficult to establish with a normal tensile test, is a significant indicator because deformation progresses in different ways during corrugation in linear sections and in sections of the maximal bend.

The mechanical test used to more fully analyze the susceptibility of low-carbon and austenitic steels to cold drawing and at the same time clearly show the uniformity of the deformation properties was the Erikson test for sheet and strip extrusion [30]. This approach was used to evaluate samples from series 1–7 that were of the same size (0.25 mm × 25 mm × 50 mm), both in the base metal zone and the welded seam zone (Figure 7).

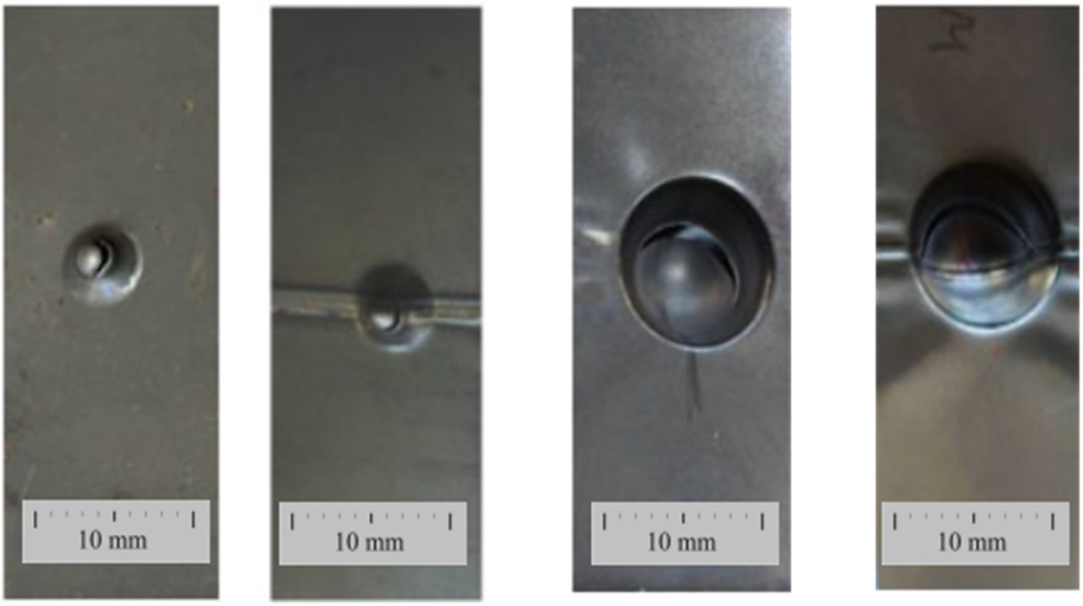

(**a**) (**b**) (**c**) (**d**)

Figure 7. The appearance of samples after the Erikson test: (**a**) base metal, (**b**) weld, punch diameter–3 mm; (**c**) base metal, (**d**) weld, punch diameter–8 mm; ×2.

Two different types of punches, measuring 3 mm and 8 mm in diameter, were used in the testing to ensure the accuracy of the findings. The results were more sensitive to the deformation conditions produced when the punch diameter was increased.

3. Results and Discussion

The dependence of the hole depth on the gas flow rate is depicted in Figure 8; the graph is based on the results of the mechanical tests using the Erikson technique. The depth of the hole is discovered to grow as the argon flow rate increases, and it almost equals to the values for the hole depths corresponding to the base metal at values of 14 to 15 lpm. The welded samples' resistance to cold plastic deformation is noticeably worse than that of the metal of the austenitic strip at shielding gas flow rates between 8 and 14 lpm.

The findings of the metallographic studies support this dependence. The success of the deformation of a thin-walled welded workpiece, i.e., a more uniform plastic flow, depends on the homogeneity of the structure, so it is crucial to obtain a finer and more uniform grain size for a thin strip, as in this case, with a thickness of 0.25 mm (a uniform grain size, a lack of pronounced liquation areas, and the absence of fragile inclusions). The presence of titanium as a modifier in the steel composition and the sufficiently quick cooling of a thin strip billet prevent the grain from growing to large sizes, but the composition's heterogeneity may well result in an uneven grain size, which may subsequently cause uneven deformation.

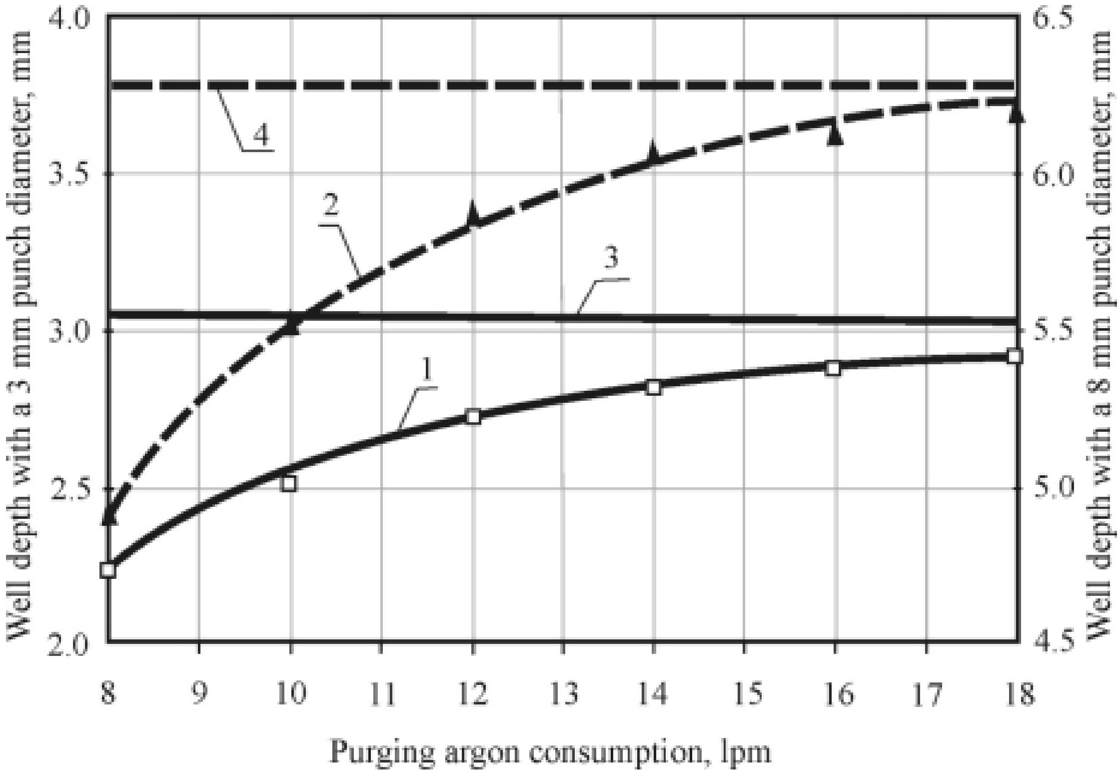

Figure 8. Influence of purging argon consumption on the results of the Erikson test: 1, 2–seam, ø 3 mm and ø 8 mm, respectively; 3, 4–base metal, ø 3 mm and ø 8 mm, respectively.

The degree of deformation, as mentioned earlier, has a dual effect on the ability of welds and the heat-affected zones to perceive mechanical loads and resist corrosion failure. During plastic deformation, an increase in the initial degree of the anodicity of the boundaries occurs due to the accumulation of deformation energy on them. In the zones of dislocation accumulation, the local anodic dissolution causes the formation of grain boundaries, areas with surface film damage, and micropits because of recently occurring damage under the action of stresses. These phenomena combined with stresses and corrosive environments cause the emergence and development of microcracks.

The metal has a greater negative potential at the depth of such damage compared to the surface areas, which accelerates the dissolution of the metal. As a result, both the stress concentration factor and the degree of the damage are increased. This creates conditions for accelerating the anodic dissolution and increasing the stress concentration to critical values preceding the development of a crack to macrosize.

A further increase in the degree of deformation, in turn, leads to energy deconcentration since the deformation areas grow to the size of a whole grain, which leads to the occurrence of reverse processes, accompanied by an increase in the corrosion resistance index. Notably, this process does not have a significant positive effect on the plastic properties of the weld metal.

The degree of deformation is further increased, and the likelihood of mechanical damage also increases, which leads to the escalation of current corrosion processes. As mentioned previously, this is caused by a rise in the second-kind stresses in local microsections and an increase in the density of dislocations. The existence of impurity concentrations and dissolved atoms, which have a higher chemical activity, causes the corrosion and sorption processes to be activated in these zones.

The properties of the base metal materials, the deformation-force scheme, and the degree and conditions of loading during manufacture, as well as the operating conditions, must all be considered in a specific analysis due to the ambiguous effect of the plastic deformation in the welded joint zone of the austenitic steel FCEs under study in the presence of structural inhomogeneity and residual thermal deformation stresses.

4. Summary

1. The current study investigated how the mode parameters affect the structure and characteristics of the welded joints of flexible compensation elements manufactured from austenitic steels. At a purging gas flow rate in the range of 16–18 lpm, an increase in the mechanical and structural properties was established. These flow rates are suggested to be used as technological recommendations in FCE production based on the research's findings.

2. Research on the microstructure of welded joints constructed of the austenitic steel grades AISI 304 and AISI 316 revealed that austenite and δ-ferrite constitute the majority of the welds and the heat-affected zone structure. Importantly, the structure of the welded joints contains the twins and chromium carbides, which precipitate at the grain boundaries. Their appearance is associated with the use of different technological processes during the production of FCE, such as molding, welding, corrugation and some others. The results of the studies demonstrate that samples of welded joints exhibited intergranular corrosion resistance at different degrees of deformation. Under certain circumstances, however, the precipitation of small particles along the grain boundaries during the manufacture of FCE can increase the sensitivity of the welded joints to intergranular corrosion, which can subsequently lead to negative effects during their operation

3. It was discovered that welds have a smoother, shinier surface with almost no discoloration along the length of the seam when the welding mode's parameters were as follows: welding current I = 14 A; welding speed v = 16 mm/s; and purging gas flow rate q = 18 lpm.

4. The study's findings show that the degree of deformation had an unclear impact on the examined steels' tendency for corrosion failure. On the one hand, an increase in the degree of deformation increases the density of dislocations and the latent energy of deformation, which, with an increase in chemical activity, results in an intensification of corrosion damage. On the other hand, the likelihood of cracking is inversely correlated with the level of inhomogeneity, even at large dislocation densities. According to the study's findings, austenitic materials should be chosen based on the degree of their deformation.

5. The Erikson extrusion testing of sheets and strips is suggested to determine the mechanical properties of the materials used in the production of welded flexible compensating elements. This method allows for the establishing of the deformation properties uniformity and the distribution of plasticity characteristics over the area of the blank.

Author Contributions: Conceptualization, E.V.L.; Methodology, V.P.I., E.V.L. and D.P.I.; Software, F.V.M.; Formal analysis, F.V.M. and V.Y.I.; Investigation, V.P.I., E.V.L., F.V.M., D.P.I. and V.Y.I.; Data curation, E.V.L. and V.Y.I.; Writing—review & editing, V.P.I., F.V.M., D.P.I. and V.Y.I.; Visualization, V.P.I. and D.P.I.; Project administration, V.P.I. and E.V.L. All authors have read and agreed to the published version of the manuscript.

Funding: This research was funded by the Government research assignment for ISPMS SB RAS grant number FWRW-2021-0003.

Data Availability Statement: Ivanov, V.; Morgay, F.; Lavrova, E.; Solidor, N. Il'yaschenko, D.P.; Verkhoturova, E.V. Investigation of the Nature of Damage to Welded Flexible Compensating Elements Made of Austenitic Stainless Steels. *Solid State Phenom.* **2021**, *328*, 9–16. Ivanov: V.; Lavrova, E.; Il'yaschenko, D.; Morgay, F.; Solidor, N. Investigation of the operational durability of high pressure metal hoses made of austenitic steels. *Solid State Phenom.* **2021**, *328*, 1–8.

Acknowledgments: The investigation of the grain structures was performed according to the Government research assignment for ISPMS SB RAS, project FWRW-2021-0003.

Conflicts of Interest: The authors declare that they have no conflicts of interest to report regarding the present study.

References

1. Ivanov, V.; Morgay, F.; Lavrova, E.; Solidor, N.; Il'yaschenko, D.P.; Verkhoturova, E.V. Investigation of the Nature of Damage to Welded Flexible Compensating Elements Made of Austenitic Stainless Steels. *Solid State Phenom.* **2021**, *328*, 9–16. [CrossRef]
2. Ivanov, V.; Lavrova, E.; Il'yaschenko, D.; Morgay, F.; Solidor, N. Investigation of the operational durability of high pressure metal hoses made of austenitic steels. *Solid State Phenom.* **2021**, *328*, 1–8. [CrossRef]
3. Krivonosova, E.A.; Rudakova, O.A.; Salamatova, E.S.; Gorchakov, A.I. Strukturnye osobennosti deformirovanija svarnyh shvov vysokolegirovannyh stalej. *Svarka I Diagn.* **2011**, *3*, 14–17.
4. Baek, J.-H.; Kim, Y.-P.; Kim, W.-S.; Young-Tai, K. Fracture toughness and fatigue crack growth properties of the base metal and weld metal of a type 304 stainless steel pipeline for LNG transmission. *Int. J. Press. Vessels Pip.* **2001**, *78*, 351–357. [CrossRef]
5. Krivonosova, E.A.; Akulova, S.N.; Myshkina, A.V. K probleme korrozionnogo razrushenija svarnyh shvov Vestnik Permskogo natsional'nogo issledovatel'skogo politekhnicheskogo universiteta. *Mashinostroenie I Materialoved.* **2017**, *3*, 114–138.
6. Burjak, T.N.; Jaroshenko, N.V.; Taranenko, A.A. Analiz materialovedcheskih aspektov v ocenke jekspluatacionnoj nadezhnosti svarnyh trub iz korrozionnostojkoj stali dlja kondensatorov AES. *Jad. Ta Radiac. Bezpeka* **2015**, *2*, 31–38.
7. García, C.; Martín, F.; de Tiedra, P.; Cambronero, L.G. Pitting corrosion behavior of PM austenitic stainless steels sintered in nitrogen–hydrogen atmosphere. *Corros. Sci.* **2007**, *49*, 1718–1736. [CrossRef]
8. Artem'eva, D.A.; Hajdorov, A.D. Vlijanie azota na korrozionnuju stojkost' hromonikelevoj stali H18N9 I H16N11M3. *Nauchno-Teh. Vedom. Cankt-Peterbg. Gos. Politeh. Univ.* **2016**, *4*, 210–222.
9. Narivskij, A.J.; Belikov, S.B. Opredelenie pittingostojkosti stali AISI 304 v hloridsoderzhashhih sredah, kotorye prisutstvujut v rabote teploobmennikov. *Fiz.-Him. Meh. Mater.* **2006**, *6*, 136–140.
10. Jun, Y.; Ming, G.; Xiaoyan, Z. Study on microstructure and mechanical properties of 304 stainless steel joints by TIG, laser and laser–TIG hybrid welding. *Opt. Lasers Eng.* **2010**, *48*, 512–517.
11. Arasappan, R.K.; Sankarapandian, S.; Pramod, R.; Shanmugam, N. Experimental and numerical studies on the influence of formability of AISI 316L tailor-welded blanks at different weld line orientations. *J. Braz. Soc. Mech. Sci. Eng.* **2021**, *43*, 171. [CrossRef]
12. Solidor, N.A.; Ivanov, V.P.; Morgay, F.V.; Nosovsky, B.I. Investigation of corrosion resistance welds metal hose made of steels AISI 304 and AISI 316. *East.-Eur. J. Enterp. Technol.* **2015**, *76*, 33–39. [CrossRef]
13. Kumar, V.; Joshi, P.; Dhakar, S. Analysis of the Effect of Sensitization on Austenitic Stainless Steel 304L Welded By GTAW Process. *IJTIR* **2015**, *14*, 2321-1814, ISBN 978-1-62951-946-3.
14. Saptarshi, S.; Mukherjee, M.; Pal, T.K. Microstructure, texture, and mechanical property analysis of gas metal arc welded AISI 304 austenitic stainless steel. *JMEPEG* **2015**, *24*, 1125–1139. [CrossRef]
15. Mukherjee, M.; Dutta, A.; Kanjilal, P.; Pal, T.K.; Sisodia, S. Enhancement of Microstructural and Mechanical Properties by Pulse Mode of Metal Transfer in Welded Modified Ferritic Stainless Steel. *ISIJ Int.* **2015**, *55*, 1439–1447. [CrossRef]
16. Karunakaran, N. Effect of Pulsed Current on Temperature Distribution and Characteristics of GTA Welded Magnesium Alloy. *IOSR-JMCE* **2013**, *4*, 1–8. Available online: www.iosrjournals.org (accessed on 21 November 2022). [CrossRef]
17. Ivanov, V.; Makarenko, N.A.; Lavrova, E.; Ahieieva, M.V. Electric Arc Deposition of an Anticorrosive Layer with Two Strip Electrodes. *Solid State Phenom.* **2020**, *303*, 39–46. [CrossRef]
18. Ghosh, A.; Bhattachraya, T.K.; Deshpande, N.V.; Basak, S. Microstructural and Mechanical Properties Analysis of Plasma ARC Welded 316L Austenitic Stainless Steel Joints without Addition of Filler Material. *Int. J. Trend Sci. Res. Dev. (IJTSRD)* **2019**, *3*, 849–865. [CrossRef]
19. Saraev, J.N.; Bezborodov, V.P.; Selivanov, J.V.; Nikonova, I.V. Vlijanie rezhimov naplavki pokrytij na korrozionnuju stojkost' v kislyh sredah svarnyh soedinenij austenitnyh stalej. *Obrab. Met.* **2007**, *2*, 33–36.
20. Ivanov, V.; Lavrova, E.; Morgay, F.; Semkiv, O. Investigation of the heat-affected zone properties during cladding of power equipment with austenitic materials using control mechanical impacts on the strip electrode. *Mater. Sci. Forum* **2021**, *1038*, 100–107. [CrossRef]
21. Unnikrishnan, R.; Idury, S.; Ismail, T.P.; Bhadauria, A.; Shekhawat, S.K.; Khatirkar, R.K.; Sapate, S.G. Effect of heat input on the microstructure, residual stresses and corrosion resistance of 304L austenitic stainless steel weldments. *Mater. Charact.* **2014**, *93*, 10–23. [CrossRef]
22. Kumar, S.; Shahi, A.S. Effect of heat input on the microstructure and mechanical properties of gas tungsten arc welded AISI 304 stainless steel joints. *Mater. Des.* **2011**, *32*, 3617–3623. [CrossRef]
23. Kuznetsov, M.A.; Kartsev, D.S.; Zhuravkov, S.P.; Barannikova, S.A. Strukturoobrazovanie i korrozionnaia stoikost' svarnykh soedinenii iz stali austenitnogo klassa. *Tekhnologii I Mater.* **2015**, *1*, 18–24.
24. Shen, J.; Gonçalves, R.; Choi, Y.T.; Lopes, J.; Yang, J.; Schell, N.; Kim, H.S.; Oliveira, J.P. Microstructure and mechanical properties of gas metal arc welded CoCrFeMnNi joints using a 308 stainless steel filler metal. *Scr. Mater.* **2023**, *222*, 115053, ISSN 1359-6462. [CrossRef]
25. Martorano, M.A.; Tavares, C.F.; Padilha, A.F. Predicting delta ferrite in stainless steel castings. *ISIJ Int.* **2012**, *52*, 1054–1065. [CrossRef]
26. Brooks, J.A.; Thompson, A.W.; Williams, J.C. A fundamental study on the beneficial effect of delta ferrite in reducing weld cracking. *Weld Res. Suppl.* **1984**, *63*, 71s–83s.
27. Taban, E.; Kaluc, E.; Aykan, T.S. Effect of the Purging Gas on Properties of 304H GTA Welds. *Weld. J.* **2014**, *4*, 124–130.

28. Bergquist, E.L.; Huhtala, T.; Karlsson, L. The effect of purging gas on 308L TIG root pass ferrite content. *Weld. World* **2011**, *55*, 57–64. [CrossRef]
29. Li, L.J.; Davis, T. Effect of purging gas oxygen levels on surface structure and mechanical properties of GTA welded Type 304 stainless sanitary tube. *J. Adv. Mater.* **2007**, *39*, 14–19.
30. *GOST R ISO 20482-2015*; Metallic Materials. Sheets and Strips. Erichsen Cupping Test. IPK Izdatel'stvo Standartov: Moscow, Russia, 2015.